Experimental MoII oscillator strengths

Sikstrom, C. M; Pihlemark, H; Nilsson, H; Litzen, U; Johansson, S; Li, Z. S; Lundberg, Hans

Published in:
Journal of Physics B: Atomic, Molecular and Optical Physics

DOI:
10.1088/0953-4075/34/3/323

2001

Experimental Mo II oscillator strengths

2001 J. Phys. B: At. Mol. Opt. Phys. 34 477

(http://iopscience.iop.org/0953-4075/34/3/323)

INSTITUTE OF PHYSICS PUBLISHING JOURNAL OF PHYSICS B: ATOMIC, MOLECULAR AND OPTICAL PHYSICS

J. Phys. B: At. Mol. Opt. Phys. **34** (2001) 477–490 www.iop.org/Journals/jb PII: S0953-4075(01)18006-5

Experimental Mo II oscillator strengths

C M Sikström[1], H Pihlemark[1], H Nilsson[1], U Litzén[1], S Johansson[1], Z S Li[2] and H Lundberg[2]

[1] Atomic Spectroscopy, Department of Physics, Box 118, 221 00 Lund, Sweden
[2] Department of Physics, Lund Institute of Technology, Box 118, 221 00 Lund, Sweden

Received 13 October 2000

Abstract

Experimental branching fractions (BFs) of Mo II, ranging in wavelength from 1970 to 4370 Å, have been measured from intensity calibrated spectra recorded with the Lund UV Fourier transform spectrometer (FTS). Radiative lifetimes for 10 levels have been measured using the method of laser-induced fluorescence (LIF). Combining BFs with new as well as previously measured lifetimes, 16 in total, oscillator strengths of 91 lines were derived. Seven transitions are resonance lines involving the ground state. The BF results are compared with calculations made with the Cowan code and the f-values are compared with previously published data. Improved wavelengths from an ongoing term analysis are also reported.

1. Introduction

The most recent analysis of the Mo II term system, performed by Kiess more than 40 years ago (Kiess 1958, Sugar and Musgrove 1988), was based on wavelength measurements of 3800 lines with uncertainties of ± 0.01 Å. Relative oscillator strengths of 58 Mo II lines were determined by Schnehage *et al* (1983), and Hannaford and Lowe (1983) measured lifetimes of 15 Mo II levels, which made it possible to put the oscillator strengths on an absolute scale. However, the investigation by Schnehage *et al* only covered the region 2700–5700 Å, which means that oscillator strengths for transitions involving the ground state were missing.

By means of Fourier transform spectroscopy (FTS) it is now possible to improve wavelength measurements to an accuracy of better than a fraction of a mÅ in the UV region. The FTS method also makes it possible to extend the analyses of complex atomic spectra, where high accuracy is needed to avoid spurious coincidences in the search for new energy levels. FTS is also well suited for intensity measurements, which can be used for determination of oscillator strengths.

The need for more accurate wavelengths and oscillator strengths mainly appears in various astrophysical research projects and is to a great extent prompted by the spectra recorded with high-resolution instruments, such as the Goddard High-Resolution Spectrograph (GHRS) and the Space Telescope Imaging Spectrograph (STIS) on-board the *Hubble Space Telescope* (HST). A good example is given by the two Mo II resonance lines that have been identified at 2015 and 2020 Å in GHRS spectra of the sharp-lined HgMn-type star χ Lupi (Brandt

0953-4075/01/030477+14$30.00

et al 1999). Only rough estimates of the oscillator strengths of these lines were available in the databases, and the laboratory wavelengths were only known to ± 0.01 Å. The existing atomic data for Mo II were thus insufficient for construction of the synthetic spectrum used for analysing the stellar spectrum.

The Mo II spectrum is now being re-investigated in a project at Lund University, using VUV Fourier transform spectrometers. The goal of the project is to provide high-precision wavelengths, to improve the accuracy of the previously known energy levels and to extend the analysis to previously unknown levels. The project also includes an experimental determination of oscillator strengths of transitions to a set of low levels, including the ground term. The result of the oscillator strength measurements is presented here, whereas the term analysis and the wavelength measurements will be reported elsewhere.

2. Experiment

The project described here is one in a series of experimental determinations of atomic oscillator strengths needed in astrophysical research. The method is based on the combination of atomic lifetimes, measured by laser-induced fluorescence (LIF) at the Lund Laser Centre (LLC), and the branching fraction (BF), determined using the Lund UV FTS instrument. A thorough knowledge of the term system of the atom or ion is necessary, to ensure that *all* transitions from an upper level are included in the BF determination. The different steps of the method will be described in the following subsections, with some emphasis on the problems related to the BFs.

2.1. Atomic structure and spectral lines of Mo II

The set of low even configurations of Mo II is $(4d+5s)^5$, i.e. $4d^5$, $4d^45s$ and $4d^35s^2$. The ground term is $4d^5\ a^6S$ with only one level, $J = \frac{5}{2}$. The second lowest even term is $4d^4(^5D)5s\ a^6D$ with five levels, $J = \frac{1}{2}$–$\frac{9}{2}$, located around 12 500 cm^{-1}. The lowest odd levels belong to the $4d^4(^5D)5p$ configuration, beginning at 45 853 cm^{-1} (see figure 1). This means that emission lines from the low odd levels with $J = \frac{3}{2}$, $\frac{5}{2}$ and $\frac{7}{2}$ may appear in two groups, resonance lines to $a^6S_{5/2}$ at roughly 2000 Å, and the rest of the lines beginning at about 600 Å longer wavelengths. For these levels, BF measurements are far more difficult than for the levels with no transitions to the ground state ($J = \frac{1}{2}$ or $J > \frac{7}{2}$), due to the influence of self-absorption and the wider wavelength region.

Mo II is homologous with Cr II (Johansson, unpublished. Most of the results are available in a NIST compilation (Sugar and Corliss 1995)) and there are large similarities between their term systems. The Mo II analysis by Kiess (1958) comprised 238 levels belonging to the $4d^5$, $4d^45s$ and $4d^45p$ configurations. In the ongoing analysis, the term system is being extended to comprise levels belonging to the $4d^45d$, $4d^46s$ and $4d^35s5p$ configurations.

The work is based on measurements of Mo II spectra emitted from a hollow cathode discharge and a Penning discharge. The spectra are recorded with an FTS instrument (Chelsea Instruments FT500), where the preliminary wavenumber scale is obtained from a He–Ne sampling laser. The final wavenumber calibration is performed by means of interferometrically measured Ar II lines (Norlén 1973). The accuracy is better than ± 5 mK for strong, symmetrical lines, which corresponds to ± 0.2 mÅ at 2000 Å. The wavelengths reported in this paper along with the f-values in tables 2 and 3 are obtained from these new measurements. It should be noted that the wavelengths of the resonance lines given by Kiess with only two decimal places are systematically (except in one case) longer by about 0.01 Å than those measured in this paper. For the rest of the lines the discrepancies are generally smaller.

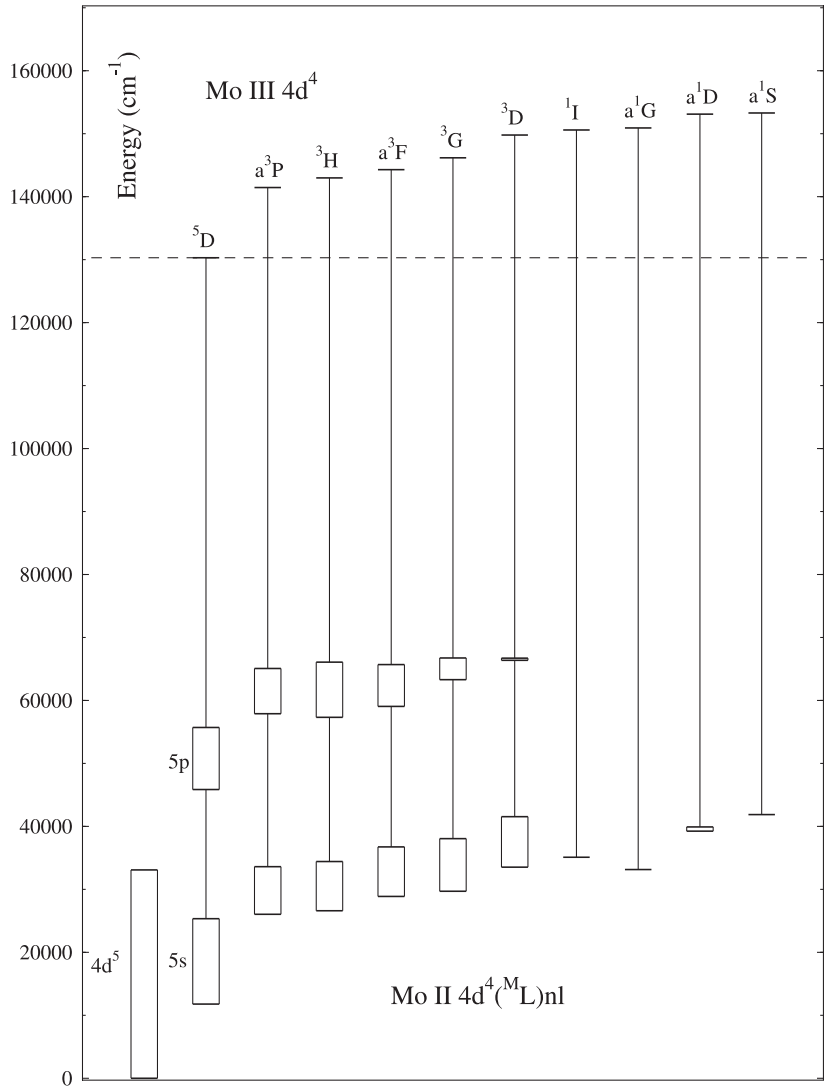

Figure 1. Partial term diagram of Mo II. Each box represents levels belonging to the same configuration and parent term. Parent term designations from Kiess (1958).

2.2. Measurements of radiative lifetimes

Time-resolved laser-induced fluorescence spectroscopy was employed for the present lifetime measurements of levels in Mo II. Selective excitation was utilized by pumping the upper levels with a tunable UV laser pulse. The temporal shape of the excitation laser pulse and the fluorescence light, released at the subsequent decay, were recorded with a fast detection system. By fitting the fluorescence signal with a convolution of the laser pulse and an exponential with a varying decay constant, reliable lifetime values were directly obtained. The technical details and experimental considerations, including figures of the experimental set-up, have been reported previously (Li *et al* 1999a, b, 2000) and only a brief description will be given here.

A Continuum Nd-60 dye laser pumped by a Continuum NY-82 Nd:YAG laser provides the laser power for excitation. The green light pulse from the Nd:YAG laser was compressed in a stimulated Brillouin scattering (SBS) compressor. This pulse was used to pump the dye laser. Operating the dye laser on the DCM dye, tunable radiation from 605 to 660 nm can be obtained. To produce the required UV radiation, frequency tripling was performed in a nonlinear crystal system, which included a KDP crystal, a retarding plate and a BBO crystal. For some levels, Raman shifting in H_2 gas of the third harmonic of the dye laser output was needed. This results in tunable UV laser radiation with a pulse duration of about 1 ns. The free Mo^+ ions were prepared in a laser-produced plasma. A green laser beam from a Nd:YAG laser was focused perpendicularly onto a rotating molybdenum target in a vacuum chamber to produce the ablation. LIF from the selected upper level was detected by a Hamamatsu 1564U microchannel-plate photomultiplier tube (200 ps rise time) after wavelength selection using a spectrometer. A digital oscilloscope, bandwidth 1 GHz and real time sampling rate 5 Gsamples/s, was used for data acquisition. To ensure a linear response of the detection system, only sufficiently weak signals were detected for each pulse and an average of 2000 pulses was performed to achieve the necessary signal-to-noise ratio. Measurements under different plasma conditions were performed to avoid systematic errors caused by collisional quenching and radiation trapping. Around 20 curves for each level have been recorded and the mean values were adopted as the final results. These are presented in table 1. The error bars reflect a more conservative view of possible residual systematic effects rather than the statistical spread of the data, which was several times lower.

The present results are compared with the results from Hannaford and Lowe (1983). As can be seen in table 1, for the levels with lifetimes longer than 4 ns, the agreement is good. However, for the short lifetime levels there is a clear discrepancy, with our values being shorter, in some cases even outside the error bars obtained by combining our errors with those reported by Hannaford and Lowe (1983). This deviation may be explained by a higher time resolution in combination with a shorter excitation pulse in our experiment. Due to the good agreement for the longer lifetimes we have not remeasured the z^6F levels, but used the Hannaford and Lowe values for deriving oscillator strengths.

2.3. Branching fractions

The branching fraction, BF, for an emission line from an upper level u to a lower level l is defined as

$$(BF)_{\mathrm{ul}} = A_{\mathrm{ul}} \Big/ \sum_k A_{\mathrm{u}k} = I_{\mathrm{ul}} \Big/ \sum_k I_{\mathrm{u}k} \tag{1}$$

where A_{ul} is the transition probability of the line and I_{ul} is the intensity measured in photons/s. $A_{\mathrm{u}k}$ and $I_{\mathrm{u}k}$ are the corresponding quantities for transitions from the same upper level, that are summed over *all* possible transitions to lower levels k.

The molybdenum spectra used to determine the BFs were emitted from a hollow cathode discharge, with the cathode consisting of a 50 mm long molybdenum tube with an inner diameter of 5 mm. Mo II lines from the low levels of the $4d^45p$ configuration appear all the way from the VUV to the visible, illustrated in figure 2. Spectra were recorded in three regions, 15 800–31 600, 19 700–39 400 and 33 000–56 000 cm^{-1}. Separate runs for these regions were necessary due to both the sensitivity of the available detectors (PMTs) and the limitations set by the effect of aliasing inherent in the FTS method. Two different Hamamatsu photomultipliers were used, R955 in the visible and near-UV regions (15 800–31 600 and 19 700–39 400 cm^{-1}) and R166, a solar blind detector, in the UV and VUV regions. The line intensities were

Table 1. Radiative lifetimes of Mo II. Energy level values and designations are taken from Kiess (1958). The measured levels have a^5D as the parent term.

Config	Term	J	Energy cm^{-1}	Lifetime (ns)	
				Expt (this work)	Hannaford and Lowe
$4d^45p$	z^6F	0.5	45 853.08		4.9(3)
$4d^45p$	z^6F	1.5	46 148.12		4.9(3)
$4d^45p$	z^6F	2.5	46 614.14		4.9(3)
$4d^45p$	z^6F	3.5	47 231.98		5.0(3)
$4d^45p$	z^6F	4.5	47 999.47		4.4(3)
$4d^45p$	z^4P	1.5	48 022.45	4.9(3)	4.8(4)
$4d^45p$	z^4P	2.5	48 860.57	2.8(2)	3.3(4)
$4d^45p$	z^6F	5.5	48 959.68		4.3(3)
$4d^45p$	z^6P	1.5	49 040.82	2.2(2)	3.0(4)
$4d^45p$	z^6P	3.5	49 481.04	2.1(2)	2.9(4)
$4d^45p$	z^6P	2.5	49 608.74	2.9(2)	3.5(4)
$4d^45p$	z^6D	0.5	49 949.45	4.3(3)	4.3(4)
$4d^45p$	z^6D	1.5	50 192.00	4.3(3)	
$4d^45p$	z^6D	3.5	50 302.54	4.0(3)	4.3(3)
$4d^45p$	z^6D	2.5	50 577.36	4.5(3)	4.7(4)
$4d^45p$	z^6D	4.5	50 705.52	4.4(3)	4.3(3)

determined as the area of Voigt functions fitted to the recorded line profiles. A calibrated deuterium lamp, in combination with known branching ratios in Ar II (Whaling *et al* 1993), was used for calibration of the observed intensities. For a more detailed description of the calibration routine see Sikström *et al* (1999b).

Self-absorption can have a major influence on the observed line intensities of resonance lines and strong transitions down to metastable levels with low excitation energies. This problem can be handled by comparing spectra with the hollow cathode lamp operated at different currents, as the amount of absorption depends on the plasma density and thus on the discharge current density. The effect of self-absorption may then be established by plotting the intensity ratio between different transitions from the same upper level to lower levels of different energies versus the current. For optically thin lines, i.e. lines with negligible absorption, these self-absorption correction curves (SACCs) will be equal to a constant function (with relative intensities not depending on the current) and no correction to the observed intensities is needed. For lines which are not optically thin, corrected intensity ratios can be derived by extrapolating the ratios to zero current.

Spectra were recorded at 10 cathode currents ranging from 150 to 1250 mA in the region 33 000–56 000 cm^{-1} where the resonance lines and the strong lines appear. In the other regions, spectra for just a few currents were recorded since no self-absorption was detected and extrapolation to zero current was not needed. Both Ne and Ar as well as a mixture of gases were tried as carrier gases at different currents.

The intensity measurement of the resonance lines was complicated by the fact that molybdenum has seven stable isotopes with mass numbers 92, 94, 95, 96, 97, 98 and 100, ranging in natural abundance between 9% and 24%. The two odd isotopes can be expected to show hyperfine structure. At low or moderate currents all line profiles appear to be symmetrical, close to Gauss functions, i.e. the isotope and hyperfine structure is too small to be observed. However, at higher currents (> 750 mA) a clear asymmetry can be seen in the profile of the strong resonance lines. This effect may be due to an isotope-dependent self-absorption. Self-

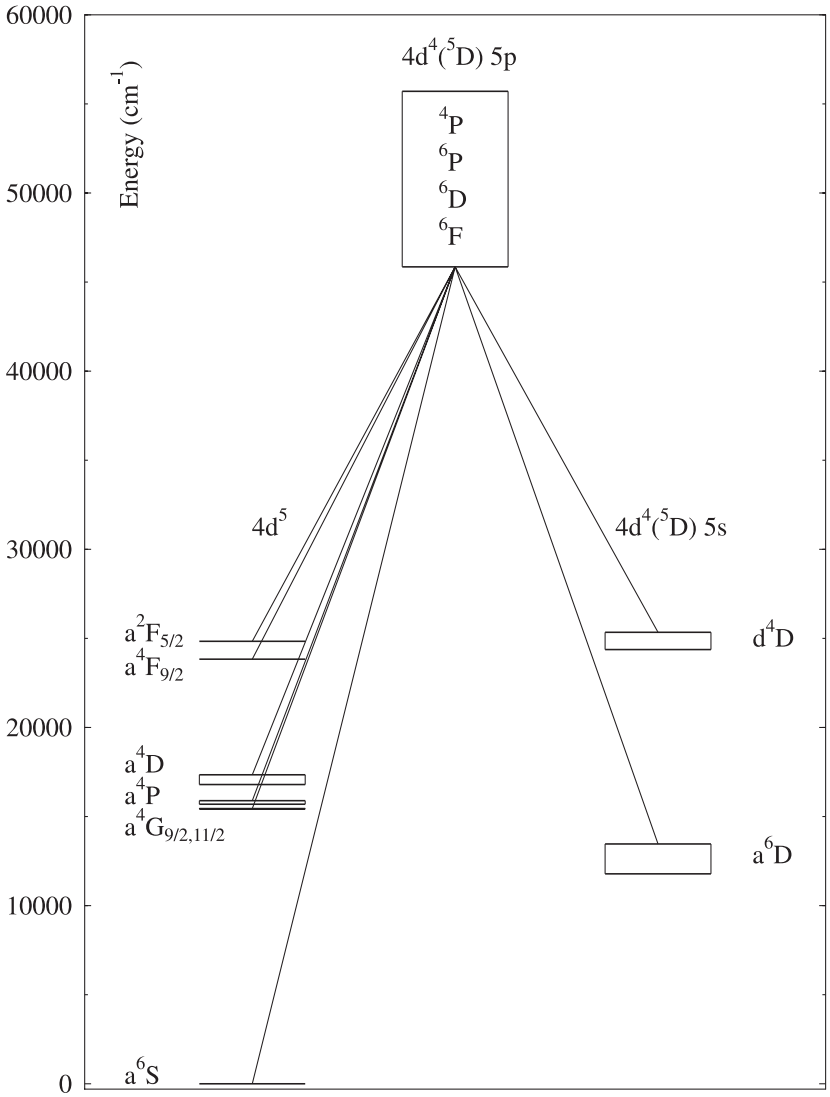

Figure 2. Term diagram of the energy levels involved in our experiment. The upper terms with levels for which lifetimes have been measured (^{4}P, ^{6}PDF) are included in the box labelled 4d^4(^{5}D) 5p. For even levels, belonging to terms where all energy levels are involved in the measured transitions, only the term designation according to Kiess (1958) is given. For the other terms, the J-values of the involved levels are given.

absorption will have a greater influence on the most abundant isotope compared with the less abundant isotopes at increasing currents, creating asymmetrical profiles. Therefore, only the lowest currents ($\leqslant 750$ mA) were used when establishing the SACCs for the resonance lines.

Only three of the lines to the term 4d^{4}5s ^{6}D, 4d^{4}5s ^{6}D$_{5/2,7/2}$–4d^{4}5p ^{6}F$_{7/2}$ and 4d^{4}5s ^{6}D$_{7/2}$–4d^{4}5p ^{6}P$_{5/2}$, showed a measurable effect of self-absorption. SACCs were derived for these lines as well, and their intensities were corrected accordingly.

To tie together the line intensities derived from spectra recorded at different spectral regions, lines present in more than one of the recorded regions were used. This is illustrated

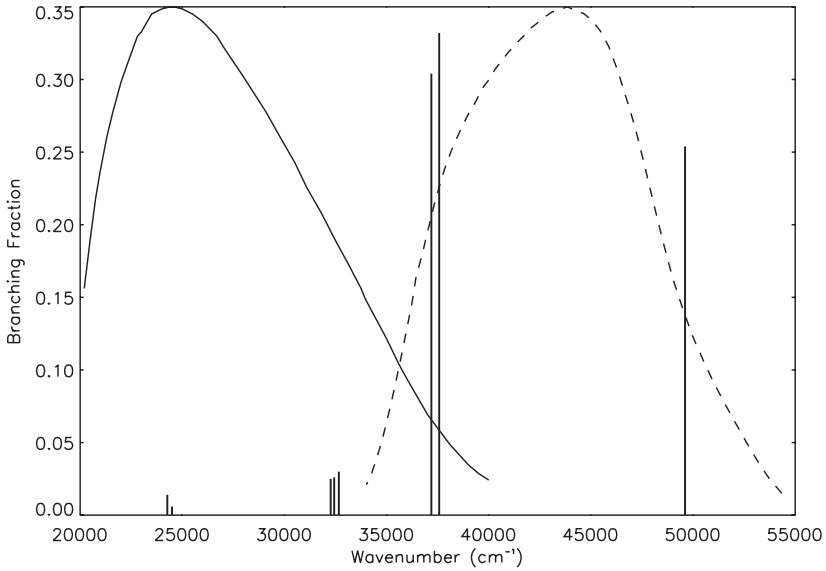

Figure 3. The figure shows the observed transitions from the upper level $4d^4 5p\ z^6P_{5/2}$, where the height of the bars corresponds to the branching fraction for each individual line. The intensity of the two lines at 37 191 and 37 574 cm^{-1} in the overlapping region was determined in both recordings. The ratio between their intensities was used to normalize the resonance line at 49 609 cm^{-1} to the lines in the 19 700–39 400 cm^{-1} region. The spectral response (in arbitrary units) of the recording 19 700–39 400 cm^{-1} is shown as the full curve and the response of the 33 000–56 000 cm^{-1} recording is shown as the dotted curve.

in figure 3. Using these lines, a ratio between the measured intensities of the recordings was established. If the same current, carrier gas and gas pressure is used, the ratio can be expected to be the same, for all lines in the overlap region, irrespective of their upper level. This implies, that in theory, it is possible to connect two different runs using only one line in the overlapping region. In practice, an average derived from several sets of lines are used to minimize the uncertainty.

3. Oscillator strengths

By using the relation

$$\tau_u = 1 \Big/ \sum_k A_{uk} \tag{2}$$

together with equation (1), the branching fraction measurements are combined with the measured lifetimes τ for deriving transition probabilities and oscillator strengths. The results, sorted by upper level, are presented in table 2.

According to equation (1) the intensities of all lines from a common upper level are needed to derive the branching fraction for a certain line from that level. Obviously a number of branches may be too weak to be observed, but the sum of their intensities may be too large to be negligible. Theoretical transition probabilities were therefore calculated to estimate the intensity of those weak lines. This was done by means of a Hartree–Fock calculation, using the Cowan computer code package (Cowan 1981), modified for PC by Ralchenko and Kramida (1995). The even configurations $4d^5$, $4d^4 5s$ and $4d^3 5s^2$ and the odd configurations $4d^4 5p$,

Table 2. Mo II branching fractions (BF) and gf-values. Lines sorted by upper level. Air wavelengths above 2000 Å.

Upper level	Lower level	λ (Å)	σ (cm^{-1})	BF Expt	BF Theory	gf Expt	Uncertainty (% in gf)
$z^6F_{1/2}$	$d^4 5s\ a^6D_{3/2}$	2956.057	33 818.97	0.218	0.209	0.117	21
	$d^4 5s\ a^6D_{1/2}$	2934.298	34 069.74	0.776	0.786	0.409	10
	Residual				0.006		
$z^6F_{3/2}$	$d^4 5s\ a^6D_{5/2}$	2963.797	33 730.65	0.130	0.115	0.139	20
	$d^4 5s\ a^6D_{3/2}$	2930.502	34 113.86	0.562	0.569	0.591	14
	$d^4 5s\ a^6D_{1/2}$	2909.117	34 364.63	0.302	0.310	0.313	19
	Residual				0.006		
$z^6F_{5/2}$	$d^4 5s\ a^6D_{7/2}$	2965.280	33 713.78	0.069	0.059	0.111	22
	$d^4 5s\ a^6D_{5/2}$	2923.392	34 196.83	0.480	0.474	0.753	16
	$d^4 5s\ a^6D_{3/2}$	2890.994	34 580.05	0.444	0.460	0.682	17
	Residual				0.007		
$z^6F_{7/2}$	$d^4 5s\ a^6D_{9/2}$	2960.242	33 771.15	0.024	0.022	0.050	23
	$d^4 5s\ a^6D_{7/2}$	2911.917	34 331.58	0.394	0.371	0.802	19
	$d^4 5s\ a^6D_{5/2}$	2871.512	34 814.64	0.575	0.600	1.138	15
	Residual				0.007		
$z^6F_{9/2}$	$d^4 5s\ a^6D_{9/2}$	2894.451	34 538.74	0.262	0.233	0.748	25
	$d^4 5s\ a^6D_{7/2}$	2848.233	35 099.17	0.732	0.762	2.025	13
	Residual				0.006		
$z^4P_{3/2}$	$d^4 5s\ b^4D_{5/2}$	4363.632	22 910.25	0.033	0.031	0.077	16
	$d^5\ a^2F_{5/2}$	4311.643	23 186.50	0.012	0.010	0.028	16
	$d^4 5s\ b^4D_{3/2}$	4279.010	23 363.32	0.040	0.031	0.090	16
	$d^5\ a^4D_{5/2}$	3258.677	30 678.45	0.029	0.021	0.038	17
	$d^5\ a^4D_{3/2}$	3240.715	30 848.49	0.100	0.067	0.128	17
	$d^5\ a^4D_{1/2}$	3201.499	31 226.34	0.040	0.029	0.051	18
	$d^5\ a^4P_{1/2}$	3111.221	32 132.40	0.012	0.010	0.014	19
	$d^5\ a^4P_{5/2}$	3092.074	32 331.36	0.179	0.116	0.210	17
	$d^4 5s\ a^6D_{5/2}$	2807.753	35 605.18	0.409	0.459	0.395	17
	$d^4 5s\ a^6D_{3/2}$	2777.854	35 988.39	0.010	0.023	0.010	26
	$d^4 5s\ a^6D_{1/2}$	2758.631	36 239.16	0.019	0.032	0.018	28
	$d^5\ a^6S_{5/2}$	2081.681	48 022.82	0.098	0.153	0.052	25
	Residual				0.017		
$z^4P_{5/2}$	$d^4 5s\ b^4D_{7/2}$	4250.697	23 518.93	0.015	0.009	0.084	20
	$d^4 5s\ b^4D_{5/2}$	4209.648	23 748.27	0.007	0.005	0.038	20
	$d^5\ a^4D_{5/2}$	3172.027	31 516.46	0.040	0.021	0.130	22
	$d^5\ a^4D_{3/2}$	3155.003	31 686.51	0.009	0.003	0.028	30
	$d^5\ a^4D_{7/2}$	3132.538	31 913.75	0.030	0.026	0.094	22
	$d^4 5s\ a^6D_{7/2}$	2780.037	35 960.14	0.508	0.425	1.263	19
	$d^4 5s\ a^6D_{5/2}$	2743.185	36 443.19	0.055	0.070	0.133	30
	$d^5\ a^6S_{5/2}$	2045.973	48 860.82	0.330	0.435	0.444	24
	Residual				0.007		
$z^6F_{11/2}$	$d^4 5s\ a^6D_{9/2}$	2816.158	35 498.93	1.000	1.000	3.320	7
	Residual				0.000		
$z^6P_{3/2}$	$d^4 5s\ a^6D_{5/2}$	2729.684	36 623.44	0.056	0.039	0.114	20
	$d^4 5s\ a^6D_{3/2}$	2701.416	37 006.65	0.232	0.224	0.462	18
	$d^4 5s\ a^6D_{1/2}$	2683.234	37 257.40	0.298	0.275	0.584	18
	$d^5\ a^6S_{5/2}$	2038.452	49 041.07	0.405	0.453	0.459	19
	Residual				0.009		

Table 2. Continued.

Upper level	Lower level	λ (Å)	σ (cm^{-1})	BF Expt	BF Theory	gf Expt	Uncertainty (% in gf)
$z^6P_{7/2}$	$d^4 5s\ a^6D_{9/2}$	2775.402	36 020.18	0.474	0.422	2.087	18
	$d^4 5s\ a^6D_{7/2}$	2732.880	36 580.61	0.062	0.065	0.263	22
	$d^4 5s\ a^6D_{5/2}$	2697.259	37 063.67	0.004	0.006	0.016	22
	$d^5\ a^6S_{5/2}$	2020.314	49 481.30	0.451	0.505	1.053	20
	Residual				0.003		
$z^6P_{5/2}$	$d^4 5s\ b^4D_{7/2}$	4119.628	24 267.19	0.014	0.012	0.075	23
	$d^4 5s\ b^4D_{5/2}$	4081.060	24 496.53	0.006	0.004	0.031	23
	$d^5\ a^4D_{5/2}$	3098.461	32 264.72	0.025	0.016	0.073	25
	$d^5\ a^4D_{3/2}$	3082.222	32 434.71	0.026	0.001	0.077	25
	$d^5\ a^4D_{7/2}$	3060.772	32 662.00	0.030	0.021	0.087	25
	$d^4 5s\ a^6D_{5/2}$	2687.992	37 191.45	0.304	0.318	0.682	30
	$d^4 5s\ a^6D_{3/2}$	2660.576	37 574.66	0.332	0.383	0.730	29
	$d^5\ a^6S_{5/2}$	2015.109	49 609.08	0.254	0.236	0.320	23
	Residual				0.009		
$z^6D_{1/2}$	$d^4 5s\ b^4D_{3/2}$	3952.973	25 290.26	0.020	0.022	0.022	25
	$d^4 5s\ b^4D_{1/2}$	3908.603	25 577.35	0.026	0.028	0.027	25
	$d^5\ a^4D_{1/2}$	3015.414	33 153.29	0.018	0.023	0.012	27
	$d^5\ a^4P_{1/2}$	2935.193	34 059.34	0.054	0.060	0.032	29
	$d^5\ a^4P_{3/2}$	2918.823	34 250.36	0.134	0.131	0.080	29
	$d^4 5s\ a^6D_{3/2}$	2636.670	37 915.33	0.532	0.558	0.258	23
	$d^4 5s\ a^6D_{1/2}$	2619.345	38 166.10	0.213	0.175	0.102	36
	Residual				0.003		
$z^6D_{3/2}$	$d^4 5s\ b^4D_{5/2}$	3986.149	25 079.77	0.030	0.031	0.066	22
	$d^5\ a^2F_{5/2}$	3942.720	25 356.02	0.010	0.010	0.022	22
	$d^4 5s\ b^4D_{3/2}$	3951.416	25 532.84	0.023	0.021	0.049	22
	$d^5\ a^4D_{5/2}$	3043.443	32 847.97	0.028	0.018	0.037	25
	$d^5\ a^4D_{3/2}$	3027.769	33 018.00	0.062	0.054	0.080	24
	$d^5\ a^4D_{1/2}$	2993.509	33 395.87	0.058	0.044	0.072	25
	$d^5\ a^4P_{1/2}$	2914.435	34 301.93	0.015	0.015	0.017	28
	$d^5\ a^4P_{5/2}$	2897.627	34 500.88	0.143	0.136	0.167	26
	$d^4 5s\ a^6D_{5/2}$	2646.486	37 774.70	0.421	0.442	0.412	25
	$d^4 5s\ a^6D_{1/2}$	2602.800	38 408.68	0.178	0.198	0.168	35
	Residual				0.032		
$z^6D_{7/2}$	$d^4 5s\ b^4D_{5/2}$	3968.651	25 190.35	0.008	0.006	0.038	26
	$d^5\ a^4D_{5/2}$	3033.232	32 958.54	0.011	0.006	0.030	28
	$d^5\ a^4G_{9/2}$	2866.541	34 875.02	0.015	0.005	0.038	32
	$d^4 5s\ a^6D_{9/2}$	2713.504	36 841.80	0.060	0.092	0.132	39
	$d^4 5s\ a^6D_{7/2}$	2672.843	37 402.22	0.433	0.439	0.928	28
	$d^4 5s\ a^6D_{5/2}$	2638.761	37 885.28	0.445	0.418	0.929	28
	$d^5\ a^6S_{5/2}$	1987.957	50 302.91	0.018	0.025	0.022	30
	Residual				0.010		
$z^6D_{5/2}$	$d^4 5s\ b^4D_{7/2}$	3961.500	25 235.82	0.092	0.095	0.290	16
	$d^4 5s\ b^4D_{5/2}$	3925.824	25 465.15	0.013	0.017	0.041	17
	$d^5\ a^2F_{5/2}$	3883.692	25 741.40	0.002	0.004	0.007	17
	$d^4 5s\ b^4D_{3/2}$	3857.196	25 918.22	0.014	0.010	0.041	17
	$d^5\ a^4D_{5/2}$	3008.149	33 233.35	0.120	0.121	0.217	20
	$d^5\ a^4D_{3/2}$	2992.839	33 403.35	0.096	0.056	0.172	20
	$d^5\ a^4D_{7/2}$	2972.611	33 630.64	0.224	0.208	0.396	18

Table 2. Continued.

Upper level	Lower level	λ (Å)	σ (cm^{-1})	BF Expt	BF Theory	gf Expt	Uncertainty (% in gf)
$z^6D_{5/2}$	$d^45s\ a^6D_{3/2}$	2653.347	37 677.03	0.264	0.285	0.372	25
	$d^45s\ a^6D_{5/2}$	2619.758	38 160.08	0.008	0.009	0.011	33
	$d^45s\ a^6D_{7/2}$	2593.710	38 543.29	0.092	0.117	0.124	31
	$d^5\ a^6S_{5/2}$	1977.155	50 577.71	0.014	0.025	0.011	32
	Residual				0.054		
$z^6D_{9/2}$	$d^45s\ b^4D_{7/2}$	3941.473	25 364.04	0.036	0.022	0.191	27
	$d^5\ a^4F_{9/2}$	3720.179	26 872.78	0.008	0.004	0.039	27
	$d^5\ a^4D_{7/2}$	2961.320	33 758.86	0.046	0.023	0.137	30
	$d^5\ a^4G_{11/2}$	2835.329	35 258.90	0.033	0.014	0.089	35
	$d^45s\ a^6D_{9/2}$	2684.140	37 244.82	0.590	0.653	1.448	22
	$d^45s\ a^6D_{7/2}$	2644.348	37 805.25	0.284	0.279	0.676	35
	Residual				0.004		

$4d^35s5p$ and $4d^25s^25p$ were included in our calculation. The final wavefunctions used were obtained by a parametric fit of the calculated energy levels to the observed ones.

The theoretical branching fractions derived from the calculated transition probabilities are presented in table 2 (BF/theory), where the branching fraction for all the lines from a common upper level that were too weak to be observed are summed and presented as 'residual'. These residuals were included in the calculation of the experimental branching fractions (BF/expt), finally used for deriving the gf values. Even though the result for individual theoretical BFs may be uncertain (for weak lines the uncertainty may be a factor of two or larger) the residuals are important for checking and correcting for missing lines.

As the theoretical calculation was carried out for the sole purpose of estimating residuals, only theoretical branching fractions and no theoretical gf-values are presented. The theoretical lifetimes tend to be shorter than those observed, probably because the possible effect of core polarization was not included in the calculation (Brage *et al* 1998, Sikström *et al* 1999a).

The uncertainty in the f-value is given in the last column of table 2 (uncertainty (% in gf)). The following sources of uncertainties were included in the determination of error bars:

(a) an uncertainty in the area determination;
(b) the uncertainty in the calibration of the deuterium lamp used for calibration in the UV region and in the calibration curve, derived from Ar II branching fractions, used in the visible and near UV;
(c) an uncertainty when applying the calibration curves to the spectra; and
(d) the uncertainty in the lifetime.

These uncertainties were added quadratically. Additionally, for lines from levels with resonance lines, it was necessary to add two additional uncertainties, namely an uncertainty in correcting for self-absorption and the uncertainty added when combining intensities from different recordings.

The final results, given as $\log gf$ in column (a), are presented in table 3, where the transitions are sorted by wavelength. The table also contains comparisons with previously published data. In the paper by Hannaford and Lowe (1983) it is suggested that the relative oscillator strengths measured by Schnehage *et al* (1983) should be put on an absolute scale by applying a normalization factor of 0.60(4). These adjusted values are listed in table 3 (column (a)) together with the arc measurements made by Corliss and Bozman (1962)

Table 3. Mo II log gf-values. Lines sorted by wavelength. Air wavelengths above 2000 Å.

λ (Å)	σ (cm^{-1})	log gf			
		Present[a]	Schnehage[b]	C&B[c]	Kuruczd[d]
1977.155	50 577.71	−1.947			
1987.957	50 302.91	−1.660			
2015.109	49 609.08	−0.495		−0.17	−1.240
2020.314	49 481.30	+0.022		+0.17	−0.900
2038.452	49 041.07	−0.338		−0.08	−1.150
2045.973	48 860.82	−0.353		−0.09	−1.160
2081.681	48 022.82	−1.283		−0.57	−1.640
2593.710	38 543.29	−0.905	−0.67	+0.49	−0.670
2602.800	38 408.68	−0.774	−0.78	+0.46	−0.780
2619.345	38 166.10	−0.991	−1.02	−0.10	−1.020
2619.758	38 160.08	−1.942			
2636.670	37 915.33	−0.589	−0.52	+0.58	−0.520
2638.761	37 885.28	−0.032	−0.07	+0.94	−0.070
2644.348	37 805.25	−0.170	−0.04	+0.89	−0.040
2646.486	37 774.70	−0.385	−0.42	+0.64	−0.420
2653.347	37 677.03	−0.429	−0.29	+0.79	−0.290
2660.576	37 574.66	−0.136	−0.22	+0.84	−0.220
2672.843	37 402.22	−0.033	−0.01	+0.95	−0.010
2683.234	37 257.40	−0.233	−0.27	+0.80	−0.270
2684.140	37 244.82	+0.161	+0.19	+1.08	+0.190
2687.992	37 191.45	−0.166	−0.25	+0.80	−0.250
2697.259	37 063.67	−1.791			
2701.416	37 006.65	−0.336	−0.37	+0.69	−0.370
2713.504	36 841.80	−0.879	−0.78	+0.40	−0.780
2729.684	36 623.44	−0.942	−0.81	+0.15	−0.810
2732.880	36 580.61	−0.580	−0.60	+0.59	−0.600
2743.185	36 443.19	−0.877			
2758.631	36 239.16	−1.743		−0.25	−1.320
2775.402	36 020.18	+0.320	+0.30	+1.33	+0.300
2777.854	35 988.39	−2.005		−0.24	−1.310
2780.037	35 960.14	+0.101		+0.97	−0.100
2807.753	35 605.18	−0.404	−0.51	+0.57	−0.510
2816.158	35 498.93	+0.521	+0.51	+1.30	+0.510
2835.329	35 258.90	−1.050		+0.11	−0.960
2848.233	35 099.17	+0.306	+0.29	+1.23	+0.290
2866.541	34 875.02	−1.421			
2871.512	34 814.64	+0.056	+0.14	+1.16	+0.140
2890.994	34 580.05	−0.166	−0.20	+0.96	−0.200
2894.451	34 538.74	−0.126	−0.15	+0.98	−0.150
2897.627	34 500.88	−0.777	−0.77	+0.33	−0.770
2909.117	34 364.63	−0.504	−0.48	+0.59	−0.480
2911.917	34 331.58	−0.096	−0.05	+0.98	−0.050
2914.435	34 301.93	−1.763			
2918.823	34 250.36	−1.098		+0.26	−0.810
2923.392	34 196.83	−0.123	−0.22	+0.98	−0.220
2930.502	34 113.86	−0.228	−0.18	+0.87	−0.180
2934.298	34 069.74	−0.388	−0.42	+0.67	−0.420
2935.193	34 059.34	−1.492		−0.00	−1.070
2956.057	33 818.97	−0.933	−1.00	+0.16	−1.000
2960.242	33 771.15	−1.303	−1.29	−0.07	−1.290
2961.320	33 758.86	−0.863	−1.09		−1.090

Table 3. Continued.

λ (Å)	σ (cm^{-1})	log *gf*			
		Present[a]	Schnehage[b]	C&B[c]	Kurucz[d]
2963.797	33 730.65	−0.856	−0.89	+0.24	−0.890
2965.280	33 713.78	−0.954	−0.75	+0.21	−0.750
2972.611	33 630.64	−0.402	−0.38	+0.66	−0.380
2992.839	33 403.35	−0.764	−0.43		−0.430
2993.509	33 395.87	−1.140	−0.98		−0.980
3008.149	33 233.35	−0.663			
3015.414	33 153.29	−1.936			
3027.769	33 018.00	−1.097	−1.03		−1.030
3033.232	32 958.54	−1.526	−1.25		−1.250
3043.443	32 847.97	−1.435			
3060.772	32 662.00	−1.062	−1.26		−1.260
3082.222	32 434.71	−1.111			
3092.074	32 331.36	−0.678		+0.37	−0.700
3098.461	32 264.72	−1.137	−1.38		−1.380
3111.221	32 132.40	−1.847			
3132.538	31 913.75	−1.028			
3155.003	31 686.51	−1.558			
3172.027	31 516.46	−0.887		+0.18	−0.890
3201.499	31 226.34	−1.297		−0.26	−1.330
3240.715	30 848.49	−0.892		−0.04	−1.110
3258.677	30 678.45	−1.422			−1.000
3720.179	26 872.78	−1.408			−1.000
3857.196	25 918.22	−1.383			−1.000
3883.692	25 741.40	−2.140			
3908.603	25 577.35	−1.564			−1.000
3925.824	25 465.15	−1.385	−1.35		−1.350
3941.473	25 364.04	−0.718	−1.83??	+0.31	−0.760
3942.720	25 356.02	−1.654			
3951.416	25 532.84	−1.312			
3952.973	25 290.26	−1.658			
3961.500	25 235.82	−0.538			−1.000
3968.651	25 190.35	−1.417	−1.18		−1.180
3986.149	25 079.77	−1.182			−1.000
4081.060	24 496.53	−1.513			
4119.628	24 267.19	−1.126	−1.27		−1.270
4209.648	23 748.27	−1.415			−1.000
4250.697	23 518.93	−1.074			−1.000
4279.010	23 363.32	−1.045			−1.000
4311.643	23 186.50	−1.554			−1.000
4363.632	22 910.25	−1.112			−1.000

[a] This work (experimental).
[b] Schnehage *et al* (1983), adjusted as recommended by Hannaford and Lowe (1983).
[c] Corliss and Bozman (1962).
[d] Kurucz database (Kurucz 1993).

(column (c)). A comparison with the Schnehage data is shown in figure 4. Finally, as a comparison, the values presently included in the Kurucz database (Kurucz 1993) are listed as well (column (d)). The Kurucz values include the data from Schnehage *et al* (1983) adjusted according to Hannaford and Lowe (1983), as seen by comparing columns (b) and (d). Where values from Schnehage *et al* were not available, adjusted values from Corliss and Bozman

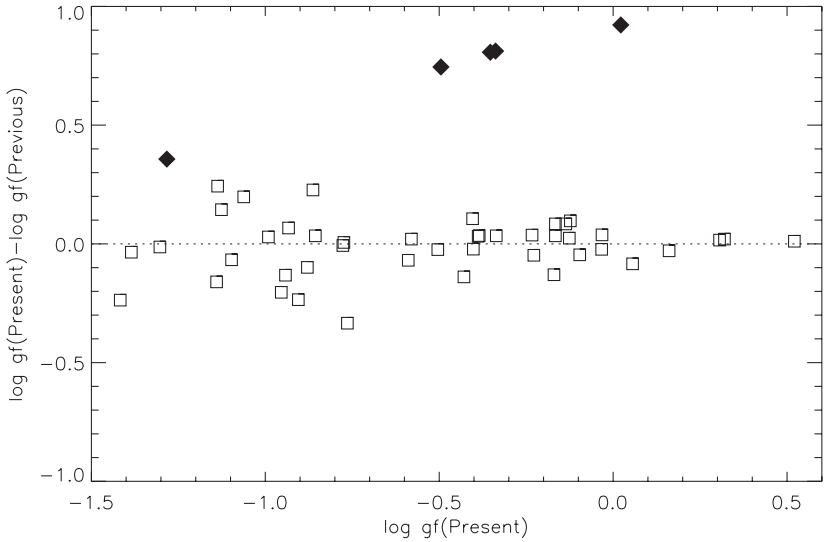

Figure 4. Comparison between our result and the values in the Kurucz database: □, derived from measurements by Schnehage *et al* (1983) adjusted as suggested in Hannaford and Lowe (1983). ♦, derived from adjusted values of the resonance lines below 2100 Å measured by Corliss and Bozman (1962). For the two resonance lines below 2000 Å (1977.155 and 1987.957 Å) no previous values are available.

(1962) were included in the database. The correction factor appears to have been derived from a comparison between the Corliss and Bozman and the Schnehage values in the region of overlap. In many cases this correction gives $\log gf$ values that are closer to our new measurements than the original Corliss and Bozman data (see, e.g., the lines at 2748, 2777 and 2780 Å). However, for the resonance lines this correction fails, meaning that the oscillator strengths previously available in the Kurucz database for these lines deviate significantly from our new results. For lines that are not present either in the Schnehage or the Corliss and Bozman tables the Kurucz values are given as $\log gf = -1.000$ with the reference 'Guess, multiplet table indicates that a line is present'.

4. Conclusions

Oscillator strengths for 91 Mo II lines were measured using the emission method. The radiative lifetime for the level $4d^4 5p\ z^6D_{3/2}$ at 50 192.00 cm^{-1} was measured for the first time and lifetimes of nine levels of Mo II were remeasured. For the shorter lifetimes, our values do not agree with the previously published values (Hannaford and Lowe 1983). For levels with $\tau > 4$ ns the agreement was found to be good.

A comparison is made between our measured f-values and the f-values published by Schnehage *et al* (1983), corrected as suggested by Hannaford and Lowe (1983). This is illustrated in figure 4. Most of the values are well within the combined experimental error bars, including the uncertainty in the lifetimes measured by Hannaford and Lowe (1983). Note that there is a large discrepancy in the gf values of the resonance lines when comparing the values presently in the Kurucz database with our results. The difference is almost one order of magnitude. This is particularly disturbing since these are lines likely to be used in abundance determinations of Mo in stars and in the interstellar medium.

References

Brage T, Wahlgren G M, Johansson S G, Leckrone D S and Proffitt C R 1998 *Astrophys. J.* **496** 1051
Brandt J C *et al* 1999 *Astron. J.* **117** 1505
Corliss C H and Bozman W R 1962 *NBS Monograph* vol 53 (Washington, DC: US Govt Printing Office)
Cowan R D 1981 *The Theory of Atomic Structure and Spectra* (Berkeley, CA: University of California)
Hannaford P and Lowe R M 1983 *J. Phys. B: At. Mol. Phys.* **16** 4539
Kiess C C 1958 *J. Res. Nat. Bur. Std.* **60** 375 RP2856
Kurucz R L 1993 *SYNTHE Synthesis Programs and Line Data* (Kurucz CD-ROM no 18) The atomic data is avaliable on the web, http://cfa-www.harvard.edu/amdata/ampdata/kurucz23/sekur.html
Li Z S, Lundberg H, Sikström C M and Johansson S 1999a *Eur. Phys. J.* D **6** 9
Li Z S, Lundberg H, Wahlgren G M and Sikström C M 2000 *Phys. Rev.* A **62** 032505
Li Z S, Norin J, Persson A, Wahlström C-G, Svanberg S, Doidge P S and Biémont E 1999b *Phys. Rev.* A **60** 198
Norlén G 1973 *Phys. Scr.* **8** 249
Ralchenko Yu V and Kramida A K 1995 Private communication
Schnehage S E, Danzmann K, Künnemeyer R and Kock M 1983 *J. Quant. Spectrosc. Radiat. Transfer* **39** 507
Sikström C M, Lundberg H, Wahlgren G M, Li Z S, Lyngå C, Johansson S and Leckrone D S 1999a *Astron. Astrophys.* **343** 297
Sikström C M, Schultz-Johanning M, Kock M, Li Z S, Nilsson H, Johansson S, Lundberg H and Raassen A J J 1999b *J. Phys. B: At. Mol. Phys.* **32** 5687
Sugar J and Corliss C 1985 *J. Phys. Chem. Ref. Data* **14** Suppl. 2
Sugar J and Musgrove A 1988 *J. Phys. Chem. Ref. Data* **17** 155
Whaling W, Carle M T and Pitt M L 1993 *J. Quant. Spectrosc. Radiat. Transfer* **50** 7